Available online at www.sciencedirect.com
SCIENCE DIRECT®
ELSEVIER
International Journal of Solids and Structures 42 (2005) 4927–4946
INTERNATIONAL JOURNAL OF SOLIDS and STRUCTURES
www.elsevier.com/locate/ijsolstr

Anisotropic elastic and elastic–plastic bending solutions for edge constrained beams

J.G. Williams [a,b], H. Hadavinia [d,*], B. Cotterell [b,c]

[a] Mechanical Engineering Department, Imperial College London, South Kensington Campus, London SW7 2AZ, UK
[b] School of Aerospace, Mechanical and Mechatronic Engineering, University of Sydney, NSW 2006, Australia
[c] Institute of Materials Research and Engineering (IMRE), 3 Research Link, Singapore 117602
[d] School of Engineering, Kingston University, Friars Avenue, London, SW15 3DW, UK

Received 9 February 2005
Available online 21 March 2005

Abstract

In beam-like fracture tests the rotation at the crack tip is a significant factor controlling the energy release rate. The local deformations of a beam ahead of the crack tip where the lower edge constrained by a stiffness is described for an anisotropic elastic material. This is a useful model for composite delamination tests and gives the crack length correction factor and root rotation which are used in determining energy release rate. The solution is calibrated using FE results and found to be accurate to within 2%.

The solution is extended by analogy to plasticity where the yielding of the constrained edge is modelled. The assumption that the deformations are controlled by the same parameters as the elastic solution is confirmed numerically. It is shown that in most practical cases the bottom edge remains elastic. This constraint is important in calculating the root rotation.

Keywords: Plastic bending; Root rotation; Plasticity; Constraint; Fracture mechanics

1. Introduction

The use of beam-like geometries in fracture tests is extensive (ISO 15024, 2001; Williams, 1993a, 1995; Kinloch et al., 1994; ESIS Peel Protocol, 2001) and covers a range from composite beam specimens (ISO 15024, 2001; ESIS Peel Protocol, 2001) to peel tests of adhered layers (Williams, 1993a; Kinloch et al.,

* Corresponding author. Tel.: + 44 2085478864; fax: +44 2085477992.
E-mail address: h.hadavinia@kingston.ac.uk (H. Hadavinia).

0020-7683/$ - see front matter © 2005 Elsevier Ltd. All rights reserved.
doi:10.1016/j.ijsolstr.2005.02.012

Nomenclature

$\bar{a}$	beam length
b	width
c	distance to the elastic–plastic interface
C	compliance
d	damage factor
E_1	axial Young's modulus of beam
E_2	transverse Young's modulus of beam
E_a	adhesive Young's modulus
G	strain-energy release-rate
h	beam depth
h_a	adhesive layer thickness
I	second moment of area
M_0	applied moment at $x = 0$
M_p	plastic collapse moment
P	applied shear force
R_0	radius of curvature of free beam at $x = 0$
R_1	radius of curvature of bonded beam at $x = 0$
R_p	radius of curvature at the onset of plasticity
S	spring stiffness
δ	end displacement of the beam
ε_Y	yield strain
ϕ	rotation factor
μ	shear modulus
ν	Poisson's ratio
θ_0	root rotation at the crack tip
σ_x	axial stress
σ_y	transverse stress
σ_Y	yield stress
τ	shear stress
Δ	characteristic length

1994). A good deal of attention has been given to the analysis (ESIS Mode II Protocol, 2001; Kanninen, 1973, 1974; Williams, 1993b) and in particular the section around the debonding point as shown in Fig. 1a. The local loading can be represented as a moment M_0 and a shear force P and for slender composite beam specimens the moment is $P\bar{a}$, where $\bar{a}$ is the beam length and $\bar{a} \gg h$ as shown in Fig. 1b. Thus the effect of the shear force, P, is slight and is a reasonable approximation to a constant moment case. For the peel test, as shown in Fig. 1c, the large deformations result in small $\bar{a}$ values and the shear force can be important. For the composites, the deformation is elastic with anisotropy and the local deformation can be analysed by various forms of beam theory (ESIS Mode II Protocol, 2001; Kanninen, 1973, 1974). For the peel test, the strips are usually isotropic but the large deformations often lead to plastic yielding which complicates the computation of energy release rates G (Williams, 1993b; Kinloch et al., 1994).

An earlier paper (Williams and Hadavinia, 2002) sought to give a consistent analysis incorporating all these effects but the plasticity case was an approximation. This paper gives the general elastic solution in a

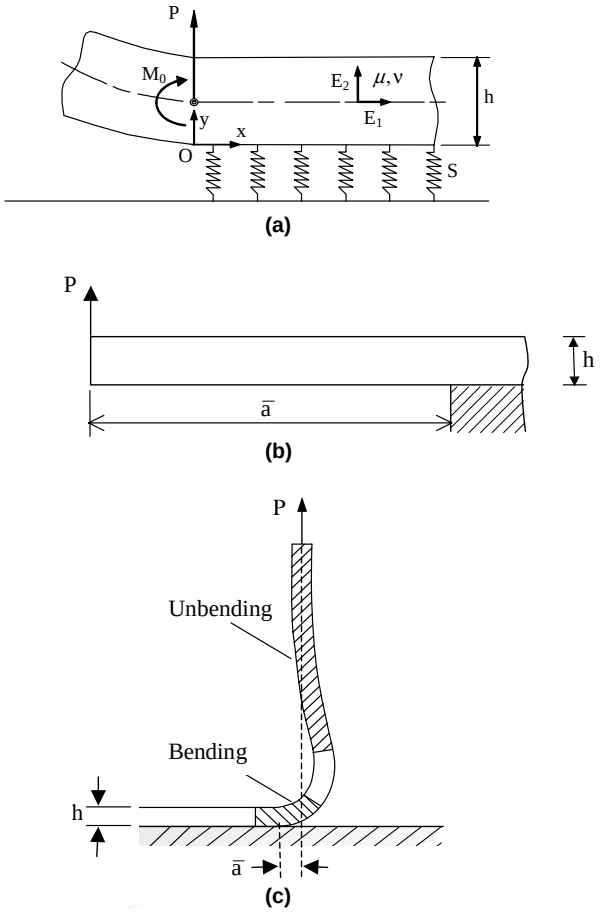

Fig. 1. Bend test geometry: (a) debond region; (b) typical composite laminate test; (c) a peel test.

form which leads naturally to the plastic case and gives a generally consistent set of results for use in G calculations.

2. The simple beam solution

The simplest solution for this problem is to use beam theory with the assumption that the bonded part of the beam is supported on a spring of stiffness S per unit width. The distributed load on the beam is thus Sv and beam theory gives

$$\frac{\mathrm{d}^4 v}{\mathrm{d}x^4} = -\frac{Sv}{E_1 I}, \quad I = \frac{h^3}{12} \text{ per unit width}$$

and E_1 is the axial modulus of the beam. For comparisons with other solutions, it is convenient to write this in terms of the moment M and since

$$\frac{\mathrm{d}^2 v}{\mathrm{d}x^2} = \frac{M}{E_1 I}$$

we have

$$\alpha_2(M''''h^4) + M = 0 \tag{1}$$

where $' = \frac{\mathrm{d}}{\mathrm{d}x}$ and $\alpha_2 = \frac{E_1}{12Sh}$.

The general solution has the form $M = A\mathrm{e}^{x/\Delta}$ and $\left(\frac{h}{\Delta}\right)^4 = -\frac{1}{\alpha_2}$, or $\left(\frac{h}{\Delta}\right) = \pm\frac{1+\mathrm{i}}{(4\alpha_2)^{1/4}}$.

Taking the real part of the solution and since $M \to 0$ as $x \to \infty$ the result is

$$M = \mathrm{e}^{-x/\Delta}(M_1 \sin x/\Delta + M_2 \cos x/\Delta) \quad \text{with } \left(\frac{\Delta}{h}\right)^4 = \frac{E_1}{3Sh} \tag{2}$$

where M_1 and M_2 are constants. The boundary conditions are

$$M = M_0 \quad \text{and} \quad M' = P \qquad \text{at } x = 0$$

and hence

$$M_1 = M_0 + P\Delta \quad \text{and} \quad M_2 = M_0$$

Also at $x = 0$ the displacement, v_0, and rotation, $\theta_0 = -v'|_{x=0}$, are given by

$$v_0 = \frac{2}{\Delta^2 S}(M_0 + P\Delta) \tag{3}$$

$$\theta_0 = \frac{2}{\Delta^3 S}(2M_0 + P\Delta)$$

The end displacement of the beam of length $\bar{a}$ is

$$\delta = 4\frac{P\bar{a}^3}{E_1 h^3} + \theta_0\bar{a} + v_0$$

and since $M_0 = P\bar{a}$ the compliance, $C = \delta/P$, is

$$C = \frac{4}{E_1 h^3}\left(\bar{a}^3 + 3\bar{a}^2\Delta + 3\bar{a}\Delta^2 + \frac{3}{2}\Delta^3\right) = \frac{4}{E_1 h^3}\left[(\bar{a} + \Delta)^3 + \frac{\Delta^3}{2}\right] \tag{4}$$

and the energy release rate is

$$G = \frac{P^2}{2}\frac{\mathrm{d}C}{\mathrm{d}\bar{a}} = \frac{6P^2(\bar{a} + \Delta)^2}{E_1 h^3} \tag{5}$$

This may be written as

$$G = \frac{6M_0^2}{E_1 h^3} + \frac{6P\Delta}{E_1 h^3}(2M_0 + P\Delta) = \frac{6M_0^2}{E_1 h^3} + P\theta_0 \tag{6}$$

This form is of particular importance in the plastically deforming case when M_0 is limited, as in the peel test, and a significant portion of G arises from the θ_0 term, which may be written as

$$\theta_0 = \left(\frac{h}{R_0}\right)\left(\chi + \frac{1}{2}\chi^2\frac{h}{\bar{a}}\right) \tag{7}$$

where $\chi = \Delta/h = (E_1/3hS)^{1/4}$ and R_0 is the radius of curvature of the free beam at $x = 0$.

The characteristic length Δ is the critical parameter in the solution and may be found via compliance, C,

$$C = \frac{4}{E_1 h^3}\left[(\bar{a} + \Delta)^3 + \frac{\Delta^3}{2}\right]$$

and if $\bar{a} \gg \Delta$, as in most composite cases, a fit to $C^{1/3}$ vs. $(\bar{a} + \Delta)$ suffices to determine Δ (Williams and Hadavinia, 2002). A good fit to data is sometimes achieved by assuming that S arises from the stiffness of the bottom half of the beam so that

$$S = 2E_2/h$$

where E_2 is the transverse modulus and hence

$$\left(\frac{\Delta}{h}\right)^4 = \frac{1}{6}\left(\frac{E_1}{E_2}\right) \tag{8}$$

which, for the isotropic case, gives $\chi = \Delta/h \approx 0.64$. This highlights the limitation of the simple bending solution since $\Delta < h$ and hence shear deformation can be an important factor. The definition of Δ can be much improved by examining the stress distributions in the bonded section.

3. Shear deformations

A useful solution may be obtained by assuming that the axial stress, σ_x, is linear in y so that

$$\sigma_x = \frac{M}{I}\left(\frac{h}{2} - y\right) \tag{9}$$

where y is measured from the bottom of the beam. Using the equilibrium equations, we may deduce the shear stress

$$\frac{\partial \tau}{\partial y} = -\frac{\partial \sigma_x}{\partial x} = -\frac{M'}{I}\left(\frac{h}{2} - y\right)$$

and

$$\tau = -\frac{M'}{2I}(hy - y^2) = -\frac{6M'}{h}(\zeta - \zeta^2), \quad \zeta = \frac{y}{h} \tag{10}$$

where $\tau = 0$ at $y = 0$ and h.

The transverse stress is given by

$$\frac{\partial \sigma_y}{\partial y} = -\frac{\partial \tau}{\partial x} = \frac{M''}{2I}(hy - y^2)$$

and assuming that $\sigma_y = 0$ at $y = h$ then

$$\sigma_y = -M''(1 - 3\zeta^2 + 2\zeta^3) \tag{11}$$

and the stress at the bottom edge is $-M''$. The anisotropic, plane stress, stress–strain relations are

$$E_1\frac{\partial u}{\partial x} = \sigma_x - v\sigma_y, \quad E_1\frac{\partial v}{\partial y} = \left(\frac{E_1}{E_2}\right)\sigma_y - v\sigma_x \tag{12a}$$

where v is Poisson's ratio, and

$$E_1\left(\frac{\partial u}{\partial y} + \frac{\partial v}{\partial x}\right) = \left(\frac{E_1}{\mu}\right)\tau \tag{12b}$$

The second of Eqs. (12a) may be integrated and v defined at $y = 0$ by the stiffness S such that

$$v|_{y=0} = \frac{\sigma_y|_{y=0}}{S} = -\frac{M''}{S} \tag{12c}$$

and hence

$$E_1 v = -M'' h\left(\frac{E_1}{E_2}\right)\left[\left(\zeta - \zeta^3 + \frac{\zeta^4}{2}\right) + \frac{E_2}{hS}\right] - \frac{6\nu M(\zeta - \zeta^2)}{h} \tag{13}$$

Eqs. (12a) and (12b) may be combined to give

$$E_1 \frac{\partial^2 v}{\partial x^2} = \frac{12M}{h^3} - \frac{6M''}{h}\left(\frac{E_1}{\mu} - \nu\right)(\zeta - \zeta^2) \tag{14}$$

Differentiating Eq. (13) and equating to Eq. (14), we have

$$\alpha_2(M'''' h^4) - \alpha_1(M'' h^2) + M = 0 \tag{15}$$

where

$$\alpha_1 = C_1\left[\frac{E_1}{\mu} - 2\nu\right]$$
$$\alpha_2 = \frac{1}{12}\left(\frac{E_1}{E_2}\right)\left[C_2 + \frac{E_2}{hS}\right]$$
$$C_1 = \frac{1}{2}(\zeta - \zeta^2), \quad C_2 = \left(\zeta - \zeta^3 + \frac{\zeta^4}{2}\right)$$

C_1 and C_2 are defined as suitable averages to give the effective shear and transverse stiffness of the beam. Cowper (1966) has explored such averages and his solution suggests that $C_1 = 1/10$, which will be used here. The simple solution, Eq. (8), effectively used $C_2 = 1/2$ but this is too large as it includes a compensation for the shear term. The results will be fitted to FE data here and $C_2 = 0.175$ is found to be a best fit.

Eq. (15) now replaces Eq. (1) for determining the characteristic length Δ and we have

$$\left(\frac{h}{\Delta}\right)^2 = \frac{1}{2\alpha_2}\left(\alpha_1 \pm \sqrt{\alpha_1^2 - 4\alpha_2}\right)$$

For low shear moduli, as in composite laminates, $\alpha_1^2 > 4\alpha_2$ and (h/Δ) has four real roots and for this case the solution has the form:

$$M = M_1 e^{-x/\Delta_1} + M_2 e^{-x/\Delta_2} \tag{16}$$

with two characteristic lengths Δ_1 and Δ_2. If we apply the same boundary conditions as in the simple bending case but using Eq. (13) to define v_0 and θ_0, i.e.

$$E_1 v = -12h(\alpha_2 M'' + \nu C_1 M)$$

we have

$$C = \frac{4}{E_1 h^3}\left[\bar{a}^3 + 3\bar{a}^2(\Delta_1 + \Delta_2) + 3\bar{a}(\Delta_1 + \Delta_2)^2 + \left(\frac{3\sqrt{\alpha_2}}{\alpha_1 + 2\sqrt{\alpha_2}}\right)(\Delta_1 + \Delta_2)^3\right] \tag{17}$$

and

$$\theta_0 = \frac{h}{R_0}\left[\left(\frac{\Delta_1 + \Delta_2}{h}\right) + \frac{1}{2}\left(\frac{\Delta_1 + \Delta_2}{h}\right)^2 \frac{h}{\bar{a}} + \frac{C_1}{2}\frac{E_1}{\mu}\frac{h}{\bar{a}}\right] \tag{18}$$

Comparison with Eqs. (4) and (7) shows that the effective characteristic length is $(\Delta_1 + \Delta_2)$ and is given by

$$\chi = \left(\frac{\Delta_1 + \Delta_2}{h}\right) = \sqrt{\alpha_1 + 2\sqrt{\alpha_2}} \tag{19}$$

For the isotropic case $\alpha_1^2 < 4\alpha_2$ and (h/Δ) is complex with two values of Δ and a form similar to Eq. (2). The results for C, θ_0 and $(\frac{\Delta_1+\Delta_2}{h})$ are the same.

It should be noted that there is an artificial discontinuity in curvature at the bond point in this solution because shear deformation is not taken into account in the free section of the beam. From Eq. (14) the radius at $x = 0$ is

$$\frac{h}{R_1} = \frac{h}{R_0}\left[1 + 2\left(1 + \frac{\chi h}{\bar{a}}\right)\frac{C_1 v + \alpha_1}{\chi^2 - \alpha_1}\right] \tag{20}$$

where the first term, h/R_0, arises from bending and the second from the shear stress effects. Eq. (18), like Eq. (7), express θ_0 in terms of h/R_0 and the change in effective Δ, i.e. $\Delta_1 + \Delta_2$, incorporates the effects of h/R_1. This point is important when considering plasticity effects which will be discussed later.

4. Comparisons with numerical solutions

Two finite element studies were performed using the FE code ABAQUS. In both a slender beam of 200 mm length and 5 mm depth with a 50 mm supported section was used with eight node isoparametric elements in plane stress. A rather course mesh with 10 elements across the beam and with a total of 2600 elements were used. Check comparisons were run with 10,000 elements and no discernible difference was found and the coarser mesh was used throughout. In the first set of data the lower edge of the supported section was fixed so that $S \to \infty$ and a wide range of E_1, E_2 and μ was used with $v = 0.3$. These values (in GPa) are listed in Table 1 together with α_1 and α_2 from

Table 1
Anisotropic solutions, $S \to \infty$, $\chi = (\frac{\Delta_1+\Delta_2}{h})$

E_1	E_2	μ	α_1	α_2	χ	χ FEA
147	7.8	0.7	20.94	0.275	4.69	4.6
147	7.8	1.4	10.44	0.275	3.39	3.34
294	7.8	2.8	10.44	0.55	3.45	3.41
147	780	2.8	5.19	2.75×10^{-3}	2.3	2.26
147[a]	7.8	2.8	5.19	0.275	2.5	2.47
73.5	7.8	2.8	2.56	0.137	1.82	1.8
147	7.8	5.6	2.56	0.275	1.9	1.88
147	7.8	11.2	1.25	0.275	1.56	1.51
147[b]	147	56.5	0.2	14.6×10^{-3}	0.66	0.66
147	7.8	22.4	0.596	0.275	1.28	1.28
147	7.8	29.1	0.445	0.275	1.22	1.21
294	7.8	29.1	0.95	0.55	1.56	1.55
588	7.8	29.1	1.96	1.1	2	2.01
147	0.78	2.8	5.19	2.75	2.91	2.91
147	0.1	2.8	5.19	21.44	3.79	3.85

$\alpha_1 = \frac{1}{10}(\frac{E_1}{\mu} - 0.6), \alpha_2 = 0.0146(\frac{E_1}{E_2})$.

[a] Typical uniaxial laminate.

[b] Isotropic case.

$$\alpha_1 = \frac{1}{10}\left(\frac{E_1}{\mu} - 0.6\right), \quad \alpha_2 = \frac{1}{12}\left(\frac{E_1}{E_2}\right)\left(0.175 + \frac{E_2}{hS}\right)$$

and $\chi = \sqrt{\alpha_1 + 2\sqrt{\alpha_2}}$. Δ was computed from compliance found from the FE results

$$\frac{\delta}{P} = C = \frac{4}{E_1 h^3}(\bar{a} + \Delta)^3$$

and the solution for the case where the plane at $x = 0$ was fixed;

$$C_0 = \frac{4}{E_1 h^3}\bar{a}^3$$

i.e.

$$\chi = \frac{\Delta}{h} = \frac{\bar{a}}{h}\left[\left(\frac{C}{C_0}\right)^{1/3} - 1\right]$$

Δ was generally of the order of 10 mm and $\bar{a}$ was 200 mm, so the error in the third power of Δ in using this approximation is small. The two values of χ are compared in Table 1 and the differences are generally less than 2%.

A similar exercise is shown in Table 2 in which the isotropic case is used and S arises from an adhesive layer of thickness h_a and modulus E_a. Thus

$$S = \frac{E_a}{h_a}$$

and

$$\alpha_1 = 0.2, \quad \alpha_2 = \frac{1}{12}\left(0.175 + \frac{h_a}{h}\frac{E}{E_a}\right)$$

In Table 2, $h_a/h = 0.1$ and E_a/E was used in the range 10^{-4} to 1 together with the value for $E_a \to \infty$. The agreement is very good for the lower ratios (i.e. 3% for $E_a/E < 0.1$). The discrepancies at higher ratios arise mostly from the effect of the adhesive layer on thickness. When $E_a/E = 1$, for example, $h = 11$ mm and the FE result should scaled to give $0.62 \times 11/10 = 0.68$, i.e. only 4% different from the analytical solution.

Overall the agreement between the FE and the analysis is good and gives confidence in the use of the analysis. The determination of Δ is part of current ISO standards for composites (ISO 15024, 2001) and comparison of the measured value with that from the elastic analysis can be useful. It has been suggested

Table 2
Adhesive layer stiffness results, $S = E_a/h_a$, $h_a/h = 0.1$, isotropic, $a_1 = 0.2$

E_a/E	χ	χ FEA
10^{-4}	4.3	4.25
10^{-3}	2.45	2.39
10^{-2}	1.43	1.39
0.05	1.03	1
0.1	0.91	0.88
0.25	0.8	0.76
0.5	0.74	0.69
0.75	0.72	0.65
1	0.71	0.62
∞	0.66	0.66

for example, (Brunner et al., 2002), that a damage factor, d, can be computed from the measured χ value by assuming that both E_2 and μ decreases by $(1-d)$ from microcracking. Thus

$$\chi^2 = \frac{1}{10}\left(\frac{E_1}{\mu(1-d)} - 2v\right) + 0.24\sqrt{\frac{E_1}{E_2(1-d)}}$$

from which d can be found.

5. Plastic deformations

At high loadings, plastic deformation may be induced in the free part of the beam which leads to energy dissipation and thus complications in computing G. This is particularly so in the peel test (Kinloch et al., 1994; Williams, 1993a). The total energy release rate available for both essential fracture work and the accompanying necessary plastic dissipation is given by

$$G = M_0\left(\frac{1}{R_0} - \frac{6M_0}{Eh^3}\right) + P\theta_0 \tag{21}$$

The necessary plastic dissipation can be calculated (Kinloch et al., 1994) but is not discussed here. We will consider first only non-work hardening. It is useful to scale the moments M_0 by that for plastic collapse, M_p, and the radius of curvature R_0, by that for the onset of plasticity R_p. Thus

$$\begin{aligned} m_0 &= \frac{M_0}{M_p}, \quad M_p = \frac{\sigma_Y h^2}{4} \\ k_0 &= \frac{R_p}{R_0}, \quad R_p = \frac{h}{2\varepsilon_Y} \end{aligned} \tag{22}$$

Introducing rotation factor ϕ, Eq. (18) becomes

$$\theta_0 = 2\varepsilon_Y k_0 \phi = 3\varepsilon_Y m_0 \phi$$

$$\phi = \chi + \left(\frac{\chi^2}{2} + \frac{(1+v)}{10}\right)\frac{h}{\bar{a}} = 0.66 + 0.35\frac{h}{\bar{a}}$$

for the isotropic elastic case ($v = 0.3$) when $S \to \infty$ and $k_0 \leqslant 1$. For an unconstrained beam for $k_0 \leqslant 1$ the elastic solution is $m_0 = 2/3k_0$ and for $k_0 \geqslant 1$, for the symmetrical yielding case,

$$m_0 = 1 - \frac{1}{3k_0^2} \tag{23}$$

A useful lower bound may be obtained by assuming that the constraint of the base is sufficient to prevent plasticity entirely so that the elastic solution prevails but the radius of curvature comes via Eq. (23), i.e.

$$\frac{\theta_0}{2\varepsilon_Y k_0 \phi} = \frac{3}{2k_0}\left(1 - \frac{1}{3k_0^2}\right) \tag{24}$$

The upper bound is given by the assumption that there is no constraint and the plasticity continues into the bonded region. In this case the curvature is the same in both sections and hence

$$\frac{\theta_0}{2\varepsilon_Y k_0 \phi} = 1 \tag{25}$$

i.e. the correction factor is the same as the elastic case. Intermediate solutions are governed by the constraint on the bottom edge which can prevent yielding and give rise to the σ_x stress distribution as shown in Fig. 2. For zero axial load, we have

$$\frac{c}{h} = \frac{2}{1+\alpha}$$

where $\alpha = \sigma_1/\sigma_Y$ and c is the distance to the elastic–plastic interface. The curvature ratio in this case is given by

$$k_1 = \left(\frac{h}{c}\right)^2 = \left(\frac{1+\alpha}{2}\right)^2 \tag{26}$$

and

$$m_0 = 2 - \frac{4}{3k_1^{1/2}} = 1 - \frac{1}{3k_0^2}$$

i.e.

$$k_1 = \left(\frac{4k_0^2}{3k_0^2+1}\right)^2 \tag{27}$$

This curvature change is in k_0 which is used to determine θ_0 in Eq. (18). A more exact curvature contains shear effects as mentioned earlier.

It is useful at this stage to return to the expression for σ_x, Eq. (9), which was the basis of the χ analysis. This may be written as

$$\sigma_x = \sigma_Y k(1-2\zeta)$$

where $k = \frac{R_p M}{EI}$ and the characteristic equation (15) is

$$\alpha_2(k''''h^4) - \alpha_1(k''h^2) + k = 0$$

and any solutions with the same form for σ_x will give the same θ_0 solutions. Thus $k = k_1$ at $x = 0$ and for the elastic and symmetrical plastic cases $k_1 = k_0$.

For the bottom edge constraint case, we have

$$\sigma_x = \sigma_Y k\left[\frac{4\alpha}{(1+\alpha)^2} - 2\zeta\right]$$

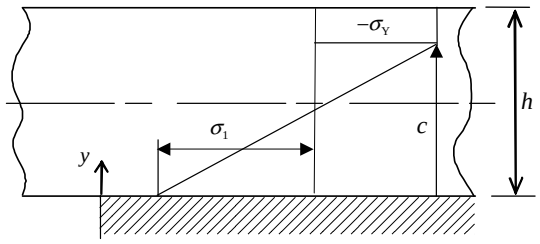

Fig. 2. Axial stress distribution with bottom edge constraint.

and for a full analogy we require that $4\alpha/(1+\alpha)^2 = 1$. This term is

$$\frac{4\alpha}{(1+\alpha)^2} = \frac{(3k_0^2+1)(5k_0^2-1)}{16k_0^4}$$

and varies slowly from 1 at $k_0 = 1$ to 15/16 at $k_0 \to \infty$. Thus we may use k_1 in place of k_0 in the elastic solution to give an approximate solution and

$$\frac{\theta_0}{2\varepsilon_Y k_0 \phi} = \frac{k_1}{k_0} = \frac{16k_0^3}{(3k_0^2+1)^2} \tag{28}$$

The limit on this constraint condition is provided by the plane strain Tresca criterion,

$$\sigma_1 > \sigma_Y + \hat{\sigma}$$

where

$$\hat{\sigma} = -M_0'' = \frac{\sigma_Y k_1}{3(\chi^2 - \alpha_1)}$$

From Eqs. (26) and (27), we have

$$\alpha = \frac{5k_0^2 - 1}{3k_0^2 + 1}$$

and for yielding,

$$\chi^2 - \alpha_1 > \frac{8k_0^4}{3(k_0^2-1)(3k_0^2+1)} \tag{29}$$

which, for the isotropic case for $\alpha_1 = 0.2$, gives $\chi > 1.04$ for $k_0 \to \infty$.

For higher values of χ, i.e. when S is low, then constrained yielding occurs on the bottom edge as shown in Fig. 3. Zero axial load now gives

$$\frac{c_1}{h} + \frac{c_2}{h} = \frac{2}{1+\alpha}$$

$$k_1 = \frac{1}{(c_2/h)^2 - (c_1/h)^2}$$

and

$$m_0 = \left(\frac{2\alpha}{1+\alpha}\right) - \frac{1}{3}\left(\frac{1+\alpha}{2}\right)^3 \frac{1}{k_1^2} = 1 - \frac{1}{3k_0^2}$$

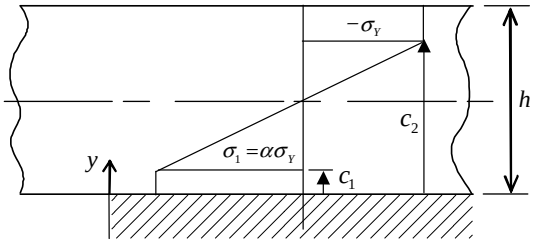

Fig. 3. Axial stress distribution for bottom edge yielding.

i.e.

$$k_1 = k_0\left(\frac{1+\alpha}{2}\right)^{3/2}\left[1+3\left(\frac{\alpha-1}{\alpha+1}\right)k_0^2\right]^{-1/2} \tag{30}$$

The α value is given by the yield criterion,

$$\alpha = 1+\frac{k_1}{3(\chi^2-\alpha_1)} = 1+\frac{k_1}{6\sqrt{\alpha_2}} \tag{31}$$

and

$$\frac{\theta_0}{2\varepsilon_Y k_0\phi} = \left(\frac{k_1}{k_0}\right)$$

The expression for the axial stress is

$$\sigma_x = \sigma_Y k_1\left[\frac{4\alpha}{(1+\alpha)^2}-2\zeta\right]$$

as before and α varies between 1 and 5/3 so again $4\alpha/(1+\alpha)^2$ varies only between 1 and 15/16.

As $\chi\to\infty$, i.e. for very low S values $\alpha\to 1$ and $k_1 = k_0$, the upper bound condition. For $\chi^2-\alpha_1 > 8/9$, Eqs. (30) and (31) may be combined to give

$$\frac{1}{k_0^2} = \frac{1}{k_1^2}\left[\frac{6(\chi^2-\alpha_1)+k_1}{6(\chi^2-\alpha_1)}\right]^3 - \frac{3k_1}{[6(\chi^2-\alpha_1)+k_1]} \tag{32}$$

and k_1/k_0 as a function of k_0 may be found for any χ value. Fig. 4 shows $\theta_0/2\varepsilon_Y k_0\phi$ for the various solutions. There are the upper and lower bounds together with the elastic base solution. The χ values marked on the elastic base solution are those at which bottom edge yielding occurs taken from Eq. (29) and it is clear

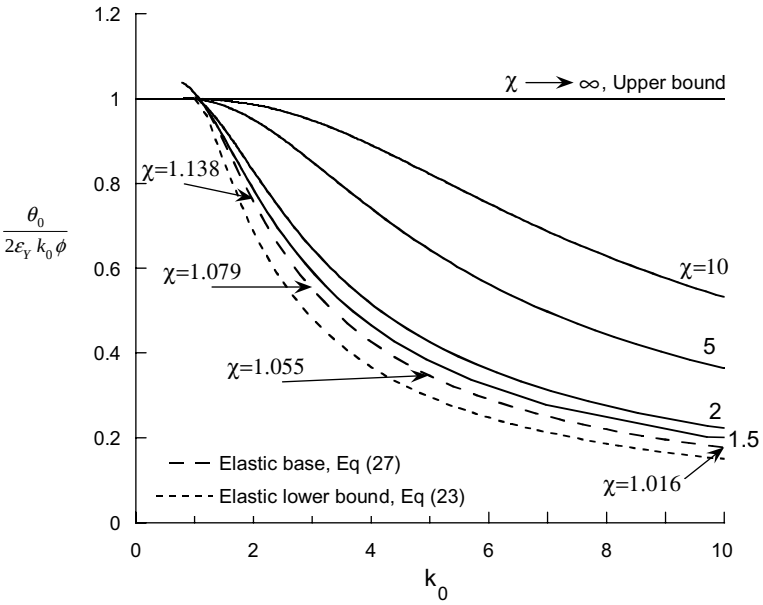

Fig. 4. Solutions for root rotations.

that the transition point is close to $k_0 = 1$ for $\chi > 1.2$. Lines from Eq. (32) are shown for $\chi = 1.5$, 2, 5 and 10 and there is significant deviation from the elastic base case for $\chi > 1.5$, i.e.

$$\frac{E}{E_a}\frac{h_a}{h} > 12$$

For typical aluminium bonded samples, for example, $h_a/h = 0.1$ and $E = 70$ GPa and so for bottom edge yielding

$$E_a < 0.6 \text{ GPa}$$

This is very low for polymer adhesives where typical values are 2–3 GPa so, in practice, the elastic base solution is likely to be the most appropriate.

Some comparison with FE results are given in Fig. 5. The geometry used was different than in the elastic case in that a shorter beam was used such that $\bar{a}/h = 6$. θ_0 was obtained directly from the slope of the central line at the crack tip and the method was checked in the elastic region to ensure that the predicted rotation factor, ϕ, was obtained. In principle it is possible to obtain R_0 and hence k_0 by taking the second derivative of the same line but the discontinuity in curvature due to shear and constraint effects at the crack tip render this direct method inaccurate. An alternative used was to determine the load and $\bar{a}$ at each point and hence the moment and then compute k_0 from Eq. (23). The code was run in plane strain so both σ_Y and E are changed, i.e. σ_Y to $\sigma_Y/(1 - v + v^2)^{1/2}$ and E to $E/(1 - v^2)$. The results are very sensitive to the value of M_p used and it was found that in the numerical data the collapsed moment was about 8% higher than the theoretical value. The reason is illustrated in Fig. 6 where the axial stress distributions are plotted for $\sigma_Y = 100$ MPa and $v = 0.3$ was used so the axial stresses should be 112.5 MPa. At a distance of 0.5h from the crack tip this is so but at the crack tip the stresses in the lower part of the beam are higher. The line

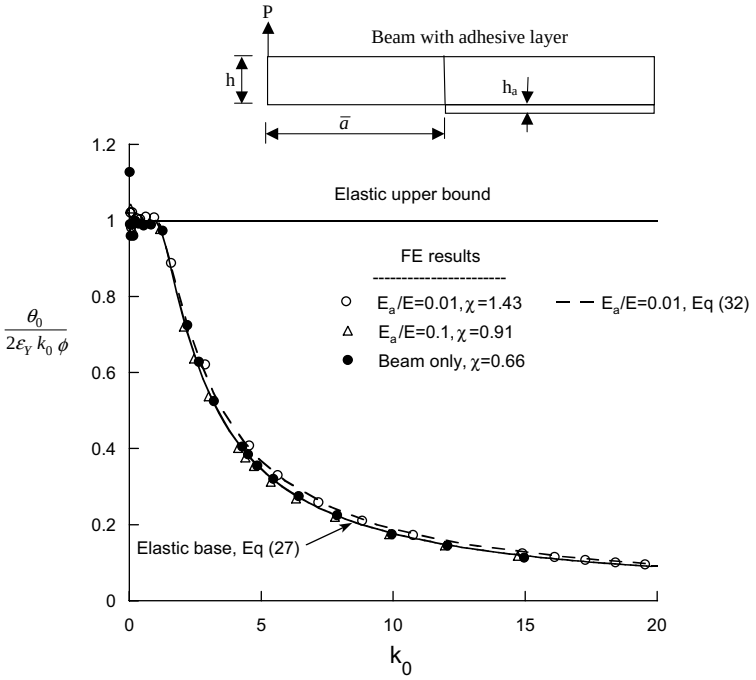

Fig. 5. Comparisons of elastic–plastic solutions with numerical data, $h_a/h = 0.1$, $\bar{a}/h = 6$ and $n = 0$.

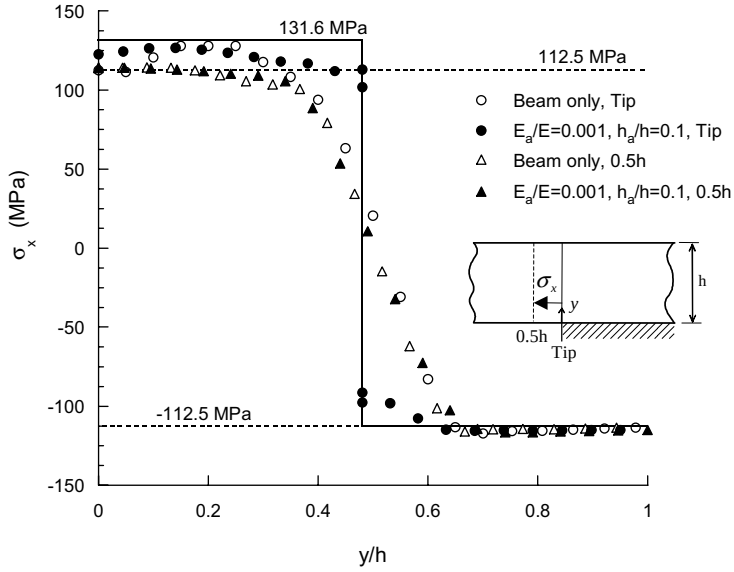

Fig. 6. Comparisons of axial stresses, $\bar{a}/h = 6$, $n = 0$.

shown is for the 8% increase which requires a stress of 131.6 MPa in the lower region. This is a consequence of local constraint and has the additional effect of moving the maximum curvature along the beam. The k_0 values in Fig. 5 are those using the moment and with M_p increased by 8%. The three cases given are for no adhesive (beam only) for which $\chi = 0.66$ ($\phi = 0.72$) and for the practical range of $E_a/E = 0.1$ and 0.01 with $h_a/h = 0.1$ giving $\chi = 0.91$ ($\phi = 0.99$) and $\chi = 1.43$ ($\phi = 1.61$), respectively. The agreement is remarkably good and confirms the validity of the various assumption used in this range. Fig. 7 shows data for two much lower stiffness, i.e. $E_a/E = 0.001$ and 0.0001. $\bar{a}/h = 6$ was used again but there were problems with

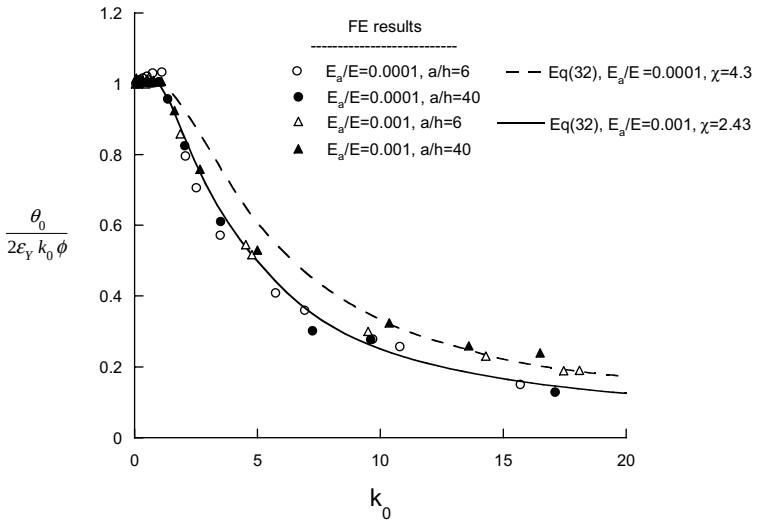

Fig. 7. Comparisons of numerical data for two different free arm length of $\bar{a}/h = 6$ and $\bar{a}/h = 40$, $h_a/h = 0.1$, $n = 0$.

numerical stability and convergence. A longer beam was also used, $\bar{a}/h = 40$, to reduce shear force effects which extended the stable range somewhat. The agreement is good for lower k_0 values (<10) for 0.001 but not as good for the higher value of 0.0001. This probably reflects the difficulty of defining k_0.

6. Work hardening

The solution may be extended to include work hardening by assuming that the strains in the elastic region extend into the two plastic zones. For the elastic, central, region the stress distribution is as in the non-work hardening case:

$$\sigma_x = \sigma_Y k(p - 2\zeta), \quad \frac{c_1}{h} < \zeta < \frac{c_2}{h} \tag{33}$$

where

$$k = \left(\frac{\alpha+1}{2}\right)\left(\frac{h}{c_2 - c_1}\right) \quad \text{and} \quad p = \left(\frac{2}{\alpha+1}\right)\left(\frac{\alpha c_2 + c_1}{h}\right)$$

To use the analogy with the elastic solution, we again require that p varies slowly in the plastic region and is close to unity.

We will use power law work hardening and in the upper plastic region we have

$$\sigma_x = \sigma_Y k^n (p - 2\zeta)^n$$

since we assume no constraint on this zone. In this range $p - 2\zeta < 0$ which models negative stresses but to avoid numerical problems for fractional powers it is preferable to use

$$\sigma_x = -\sigma_Y k^n (2\zeta - p)^n, \quad \frac{c_2}{h} < \zeta < 1 \tag{34}$$

in this range. For the lower region, we have

$$\sigma_x = \sigma_Y \alpha^{1-n} k^n (p - 2\zeta)^n, \quad 0 < \zeta < \frac{c_1}{h} \tag{35}$$

Note that at $\zeta = c_2/h$, $\sigma_x = -\sigma_Y$ and at $\zeta = c_1/h$, $\sigma_x = +\alpha\sigma_Y$.

The yield criterion at $\zeta = c_1/h$ is given by

$$k_1 = 3(\alpha - 1)(\chi^2 - \alpha_1) \tag{36}$$

The zero end load condition gives a relationship between p and k_1, i.e.

$$\alpha^{1-n} p^{1+n} - (2 - p)^{1+n} = \left(\frac{1-n}{2}\right)(\alpha^2 - 1)\frac{1}{k_1^{1+n}} \tag{37}$$

and k_0 is found from the moment expression at $x = 0$ where $k = k_1$;

$$\begin{aligned} m_0 &= \frac{2}{2+n}\left\{(2-p)^{1+n}k_1^n - \left(\frac{1-n}{3}\right)\left[\left(\frac{\alpha^3+1}{2}\right)\frac{1}{k_1^2} - \frac{3}{4}(\alpha^2-1)\frac{p}{k_1}\right]\right\} \\ &= \frac{2}{2+n}\left[k_0^n - \left(\frac{1-n}{3}\right)\frac{1}{k_0^2}\right] \end{aligned} \tag{38}$$

Solutions for k_1 as a function of k_0 may be found for a given value of χ by choosing an α value ($\alpha_1 > 1$) and computing k_1 from Eq. (36). p is found from Eq. (37) and then k_0 from Eq. (38). Fig. 8 shows the solution for $n = 0.2$ and $\alpha_1 = 0.2$, equivalent to that in Fig. 4 for $n = 0$ and in Fig. 9 p is shown to decrease to about 0.8 at $k_0 = 20$.

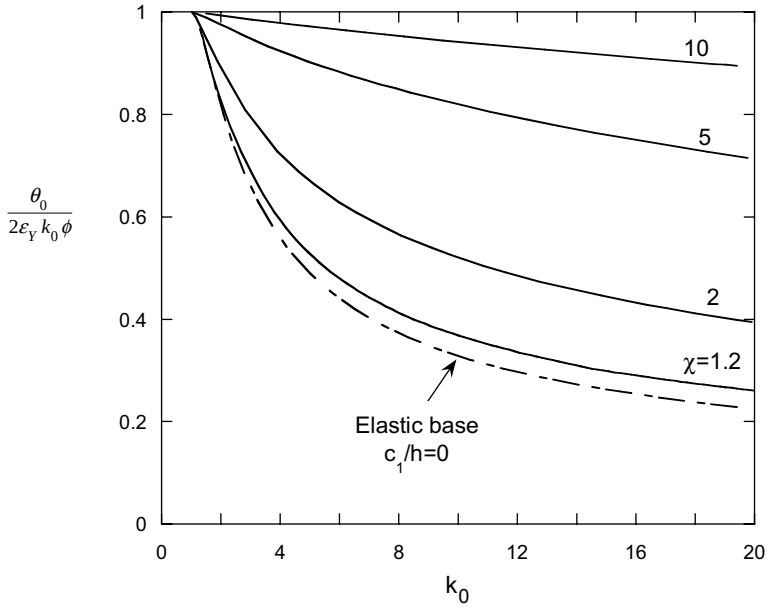

Fig. 8. Solutions for root rotation, $n = 0.2$ and $\alpha_1 = 0.2$.

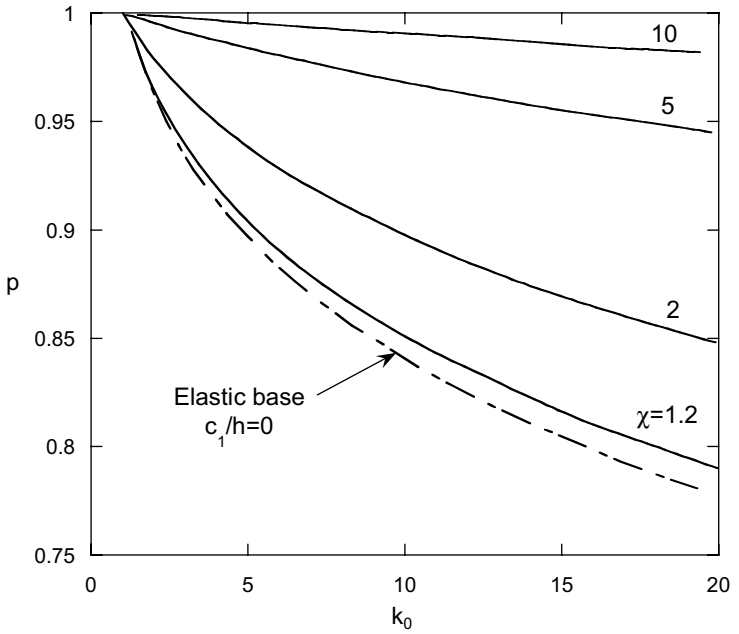

Fig. 9. Stress distribution parameter p, $n = 0.2$ and $\alpha_1 = 0.2$.

The elastic base solution is most easily retrieved by taking $c_1/h = 0$ which gives

$$pk_1 = \alpha$$

and p is then an explicit function of α. From Eq. (37),

$$p = \frac{2\alpha}{\alpha + \left[1 + \left(\frac{1+n}{2}\right)(\alpha^2 - 1)\right]^{1/1+n}} = \frac{\alpha}{k_1} \tag{39}$$

and again k_0 may be found from Eq. (38). The limiting values of χ for this case are given by Eq. (36)

$$\chi^2 = \alpha_1 + \frac{k_1}{3(\alpha - 1)} = \alpha_1 + \frac{1}{6(\alpha - 1)}\left\{\alpha + \left[1 + \left(\frac{1+n}{2}\right)(\alpha^2 - 1)\right]^{\frac{1}{1+n}}\right\}$$

For $n = 0$ we retrieve Eq. (29) and for $n = 1$,

$$\chi^2 = \alpha_1 + \frac{k_0}{3(k_0 - 1)} \tag{40}$$

Fig. 10 shows χ as a function of k_0 for $\alpha_1 = 0.2$ for these two cases which both tend to asymptotes as $k_0 \to \infty$; i.e. 1.04 for $n = 0$ and 0.73 for $n = 1$. Other values of n give intermediate curves with very flat minima as shown for $n = 0.2$ and 0.5. Thus no degree of work hardening will induce lower edge yielding for the $S \to \infty$ case when $\chi = 0.66$. A further parameter of interest is shown in Fig. 11 where p for the elastic base case, the minimum, is shown as a function of n for a range of k_0 values. For $n = 0$ the lower limit of p is $15/16 = 0.94$ and for $n = 1$, $p = 1$. Thus in the extreme cases the elastic analogy is reasonably accurate but the variations in p are up to 25% for $n \approx 0.4$. The highest practical values are about 0.2 and the solutions are likely to be less accurate than the $n = 0$ case. The solution can be corrected for values

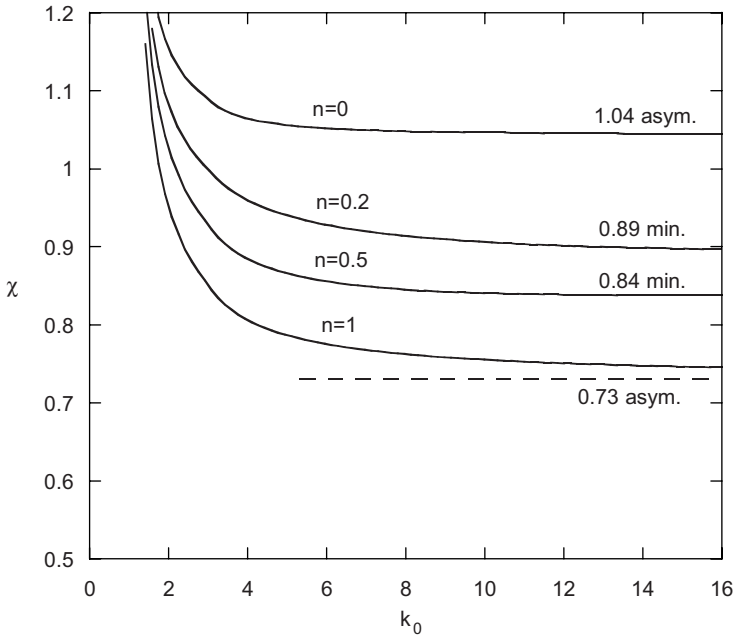

Fig. 10. Limiting value of χ for lower edge yielding, $\alpha_1 = 0.2$.

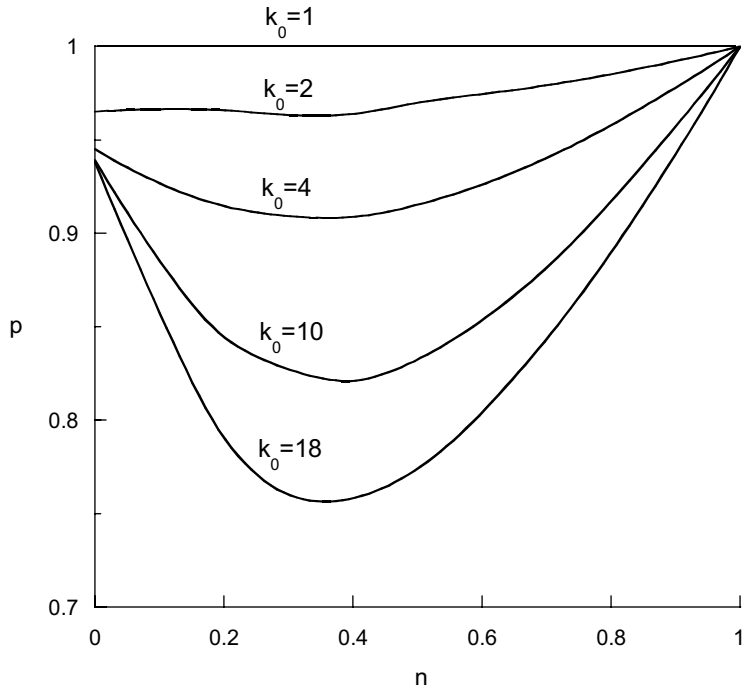

Fig. 11. Stress distribution parameter p as a function of n for the elastic base case.

of p other than unity by re-deriving the characteristic equation to give α_1 and α_2 for this case. These may be approximated to

$$\alpha_1 = 2C_1 + (1-p) \quad \text{and} \quad \alpha_2 = \frac{(4-3p)}{12}\left(C_2 + \frac{E}{hS}\right)$$

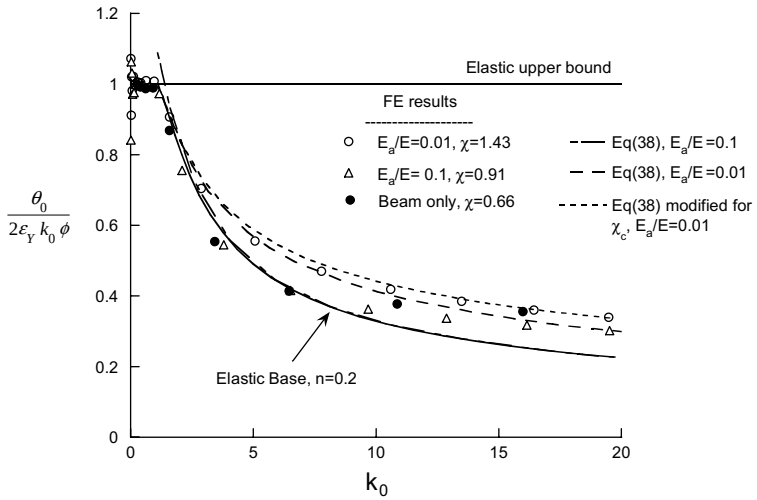

Fig. 12. Comparisons of elastic–plastic solutions with numerical data, $h_a/h = 0.1$, $\bar{a}/h = 6$, $n = 0.2$.

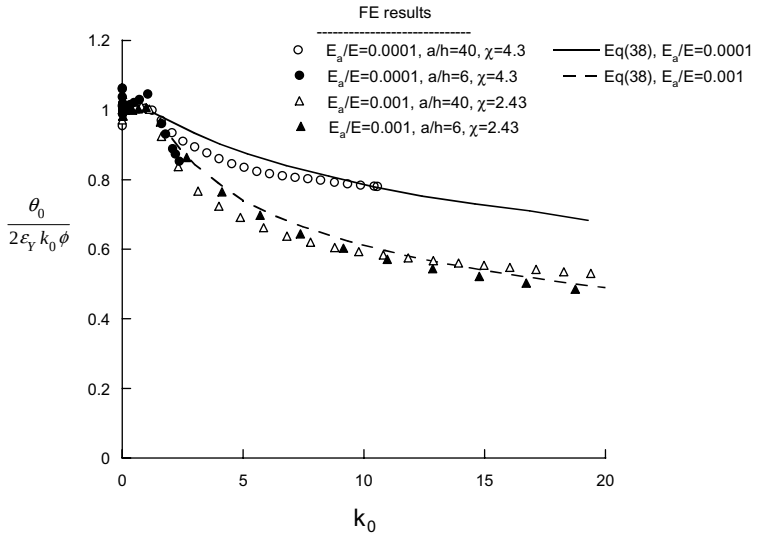

Fig. 13. Comparisons of numerical data for two different free arm length of $\bar{a}/h = 6$ and $\bar{a}/h = 40$, $h_a/h = 0.1$, $n = 0.2$.

for the isotropic case. Thus a corrected value of χ, χ_c, may be computed from

$$\chi_c^2 = (1.2 - p) + (4 - 3p)^{1/2}(\chi^2 - 0.2) \tag{41}$$

For $n = 0$ the lowest value of χ, 0.66, becomes 0.72, i.e. about 10% change. For $n = 0.2$ the changes are about 30% for the higher k_0 values. Such corrections are worthwhile but do not, of course, give an exact solution since p is assumed to be constant.

Fig. 12 shows numerical data for the same practical range of values as in Fig. 5 but this time for $n = 0.2$. k_0 is again found via the moment with M_p increased by 8%. The agreement with analytical results is good for $k_0 < 10$ but there are discrepancies at higher values, particularly for the beam only case. This is probably due, again, to the difficulty in defining k_0. For $E_a/E = 0.01$, χ was modified to χ_c using Eq. (41), as shown, but the difference is small. Given the approximate nature of the analytical solution the agreement is judged to be satisfactory. Fig. 13 gives results for the two low adhesive modulus cases and reasonable agreement is apparent.

7. Conclusions

The modification of the simple beam theory to include transverse and shear stresses give satisfactory results when compared to FE data over a wide range of anisotropic elastic properties. It is of particular note that the low shear stiffness, which is common in laminates, is accurately modelled.

The extension of the analysis to elastic–plastic yielding by analogy with the elastic solution is also successful. This essentially assumes that the deformations are determined by the elastic section and are unaffected by the plasticity. The loss of symmetry in the axial stress distribution in the bonded region does not appear to have a significant effect which is why the analogy works. Again comparison with FE data is good for the non-work hardening and the work hardening though the latter is less accurate. A similar analysis using cohesive zone models and limiting stresses is given in Cotterell et al. (in press).

Acknowledgment

The authors wish to acknowledge financial support via a collaborative programme between IMRE and Imperial College London and from the Engineering Physical Science Research Council of UK through a Platform Grant Award (HH, JGW). Part of the work was performed in the University of Sydney (BC, JGW).

References

Brunner, A.J., Blackman, B.R.K., Williams, J.G., 2002. Fracture of Polymer, Composites and Adhesives II. Elsevier.

Cotterell, B., Hbaieb, K., Williams, J.G., Hadavinia, H., Tropsa, V., in press. The root rotation in double cantilever beam and peel tests. Mech. of Mat.

Cowper, E.R., 1966. J. Appl. Mech. 33, 335.

ESIS, Mode II Protocol, 2001. In: Moore, D.R., Pavan, A., Williams, J.G., Fracture Mechanics Testing Methods for Polymers Adhesives and Composites. ESIS Publication 28, Elsevier.

ESIS Peel Protocol, 2001. In: Moore, D.R., Pavan, A., Williams, J.G., Fracture Mechanics Testing Methods for Polymers Adhesives and Composites. ESIS Publication 28, Elsevier.

ISO 15024, 2001. Standard test method for mode I interlaminar fracture toughness, G_{Ic}, of unidirectional fibre-reinforced polymer matrix composites.

Kanninen, M.F., 1973. An augmented double cantilever beam model for studying crack propagated and arrest. Int. J. Fract. 9, 83–92.

Kanninen, M.F., 1974. A dynamic analysis of unstable crack propagation and arrest in the DCB test specimen. Int. J. Fract. 10 (3), 415–431.

Kinloch, A.J., Lau, C.C., Williams, J.G., 1994. The peeling of flexible laminates. Int. J. Fract. 66, 45–70.

Williams, J.G., Hadavinia, H., 2002. Elastic and elastic–plastic correction factors for DCB specimens. In: 14th European Conference in Fracture ECF14, Cracow, EMAS Publishing, vol. 3, pp. 573–592.

Williams, J.G., 1993a. A review of the determination of energy release rates for strips in tension and bending. Part I—static solutions. J. Strain Anal. 28, 237–246.

Williams, J.G., 1993b. Root rotation and plastic work effects in the peel test. J. Adhesion 41, 225–239.

Williams, J.G., 1995. Fracture in adhesive joints: the beam on elastic foundation model. In: ASME Symposium on Mechanics of Plastics and Plastics Composites, San Francisco, USA.